HEALTH AND MEDICINE

Ultraefficient extracellular vesicle–guided direct reprogramming of fibroblasts into functional cardiomyocytes

Hyosuk Kim[1]†, Byeong-Wook Song[2]†, Soon-Jung Park[3], Seong Woo Choi[3], Hanbyeol Moon[2], Ki-Chul Hwang[2], Sun-Woong Kang[4], Sung-Hwan Moon[2], Yoosoo Yang[1], Ick Chan Kwon[1,5,6]*, Sun Hwa Kim[1]*

Direct lineage conversion holds great promise in the regenerative medicine field for restoring damaged tissues using functionally engineered counterparts. However, current methods of direct lineage conversion, even those using virus-mediated transgenic expression of tumorigenic factors, are extremely inefficient (~25%). Thus, advanced methodologies capable of revolutionizing efficiency and addressing safety concerns are key to clinical translation of these technologies. Here, we propose an extracellular vesicle (EV)–guided, nonviral, direct lineage conversion strategy to enhance transdifferentiation of fibroblasts to induced cardiomyocyte-like cells (iCMs). The resulting iCMs have typical cardiac Ca^{2+} transients and electrophysiological features and exhibit global gene expression profiles similar to those of cardiomyocytes. This is the first demonstration of the use of EVs derived from embryonic stem cells undergoing cardiac differentiation as biomimetic tools to induce cardiac reprogramming with extremely high efficiency (>60%), establishing a general, more readily accessible platform for generating a variety of specialized somatic cells through direct lineage conversion.

INTRODUCTION

Direct lineage conversion (or reprogramming) of somatic cells from one specialized type to another without entering a pluripotent state offers a game-changing strategy for future regenerative medicine applications. This approach is potentially safer and faster than those using induced pluripotent stem cells (iPSCs) as an intermediate step to generate the desired cell type (*1*). In particular, direct cell conversion technologies are useful for augmenting cardiac repair and regeneration, since the loss of cardiomyocytes could theoretically be compensated by directly reprogramming resident cardiac fibroblasts, the most abundant noncardiomyocyte cell type (~60%) in hearts (*2*). Current protocols for direct cardiac reprogramming rely on virus-based transgene expression systems to overexpress defined transcription factors (e.g., Oct4 and Klf4) that promote stem-like and tumorigenic traits (*3*, *4*). Despite inherently high transfection efficiencies of viral methods such as transgene activation, associated safety concerns relating to residual expression and insertion-mutagenesis impose severe limitations on their clinical applications (*5*). Nonviral, transgene-free, small molecule–driven approaches have recently been extensively investigated as a strategy for improving safety profiles of reprogramming techniques (*3*, *4*). In addition, select microRNA (miRNA) clusters have been used to carry out direct cell reprogramming without the involvement of exogenous transcription factors (*6*, *7*). Because of the possibility that a single miRNA can regulate multiple transcripts, it is thought that a cluster of miRNAs would act synergistically to induce cellular reprogramming by modulating an enormous number of targets. To date, however, most nonviral and transgene-free methods have yielded poor reprogramming efficiency (table S1), falling short of the bare minimum necessary to produce the desired pharmacological effects. Thus, developing nontransgenic direct lineage conversion techniques that provide a revolutionary enhancement in reprogramming efficiency remains a challenge.

To address this, we here introduce extracellular vesicle (EV)–guided, direct lineage conversion method for inducing transdifferentiation of fibroblasts into functional cardiomyocytes (Fig. 1). Cell-derived EVs have recently been used to promote the differentiation of stem cells into various mature somatic cell types, predominantly through transferred EV miRNAs (*8*). Since the discovery that EVs can lead to phenotypic changes in target cells, several studies have revealed the functions of EVs in cell differentiation and reprogramming (*9*). In addition to their capacity to carry functional biomolecules, EVs, by virtue of their phospholipid-based envelopes, also offer the advantage of readily crossing the plasma membrane of recipient cells, a critical step in cell reprogramming that appears to pose limits for viral vectors. In this study, we found that EVs separated from embryonic stem cells (ESCs) undergoing cardiac differentiation were capable of inducing direct conversion of mouse embryonic fibroblasts (MEFs) to cardiomyocytes with markedly increased reprogramming efficiency (>60%). We thoroughly optimized the protocol for EV-guided direct lineage conversion using a stepwise induction strategy to transdifferentiate fibroblasts into electrophysiologically functional cardiomyocytes. The optimized reprogramming conditions produce clusters of beating induced cardiomyocyte-like cells (iCMs) ~3-fold more efficiently than conventional methods. Because this strategy passes through the cardiac precursor stage rather than the pluripotent state, it shortens the time required to complete the conversion process. The resulting cardiac progenitor–like cells

[1]Center for Theragnosis, Biomedical Research Institute, Korea Institute of Science and Technology (KIST), Seoul 02792, Republic of Korea. [2]College of Medicine, Institute for Bio-Medical Convergence, Catholic Kwandong University, Gangneung-si 25601, Republic of Korea. [3]Department of Stem Cell Biology, School of Medicine, Konkuk University, Seoul 05029, Republic of Korea. [4]Predictive Model Research Center, Korea Institute of Toxicology, Daejeon 34114, Republic of Korea. [5]KU-KIST Graduate School of Converging Science and Technology, Korea University, Seoul 02841, Republic of Korea. [6]KIST-DFCI ON-SITE-LAB, Department of Cancer Biology, Dana Farber Cancer Institute, Boston, MA 02215, USA.
*Corresponding author. Email: ikwon@kist.re.kr (I.C.K.); sunkim@kist.re.kr (S.H.K.)
†These authors contributed equally to this work.

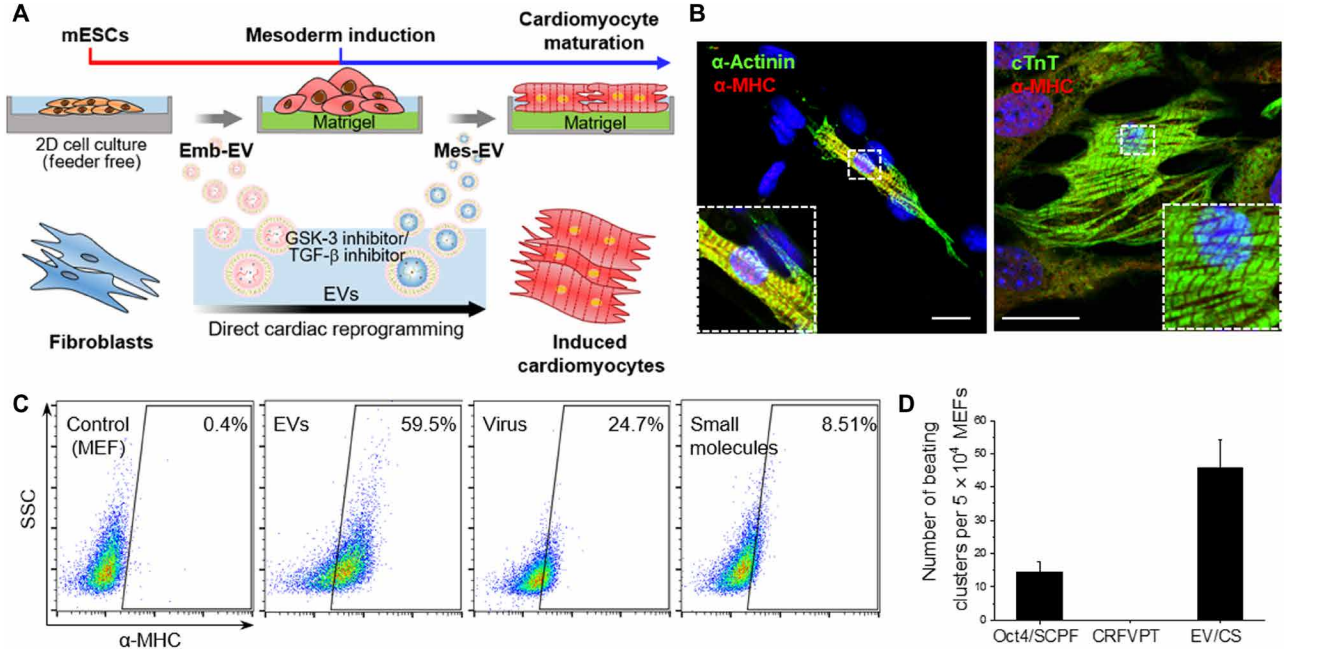

Fig. 1. Direct conversion of fibroblasts into functional cardiomyocytes. (**A**) Schematic illustration of EV-guided direct cardiac reprogramming. (**B**) Sarcomeric structure revealed by immunostaining for α-MHC, cTnT, and α-actinin in single cells digested from iCM beating clusters. Scale bars, 40 μm. (**C** and **D**) Comparison of cardiac reprogramming efficiency with that of previously described protocols. (C) Fluorescence-activated cell sorting (FACS) analyses of α-MHC$^+$ cells at day 20 in EV/CS, virus (Oct4/SCPF), and small molecule (CRFVPT) groups. Abbreviations of small molecules are provided in table S2. (D) Number of beating clusters at day 20 in OCT4/SCPF, CRFVPT, and EV/CS groups.

could be further differentiated into smooth muscle cells and endothelial cells in addition to cardiomyocytes. Our EV-guided direct cardiac reprogramming method offers great promise to promote cardiac healing and restore cardiac function after an insult.

RESULTS AND DISCUSSION

Establishment of a serum-free 2D-directed differentiation system and characterization of EVs derived from cardiomyocyte differentiation process

Before establishing direct conversion conditions using EVs, we first optimized a feeder-free culture system for ESCs. It is important that only EVs separated from differentiating ESCs be used, avoiding those derived from serum or feeder cells (e.g., MEFs); this is a potential issue because a variety of EVs are present in fetal bovine serum (FBS) products used for cell culture (*10*). To obtain accurately and precisely processed EVs from ESCs undergoing cardiac differentiation, we used a serum-free two-dimensional (2D)–directed differentiation system (fig. S1A). Using this method, we observed spontaneous beating cardiomyocytes from day 6. On day 15 after differentiation, a fluorescence-activated cell sorting (FACS) analysis showed that >85% of cells were positive for cardiac troponin T (cTnT), a cardiac-specific marker (fig. S1B), indicating that our system promotes the differentiation of the vast majority of ESCs to the specialized cell type, exhibiting an efficiency comparable to that previously reported (*11*–*14*). In addition, since dying cells could contribute to EV-like particles in culture and contaminate EV contents (*15*, *16*), the rate of cell death was measured at each stage of differentiation (fig. S1C). EVs present in the medium from the first stage of differentiation [EB (Embryoid body) formation] to the stage before mesodermal induction were termed Emb-EV, and those in the medium after the mesodermal induction stage were named Mes-EV. The separated EVs were characterized in terms of size, morphology, and EV markers (fig. S2, A to C). The mean particle diameter measured by dynamic light scattering (DLS) analysis ranged from 70 to 90 nm. Cryogenic transmission electron microscopy (TEM) revealed the expected globular-shaped membrane vesicles and lipid bilayers. Since tetraspanins (CD9, CD81, and CD63) and multivesicular body biogenesis proteins (TSG101) were inserted in the membrane surface of EVs or identified most frequently in EVs, they are generally accepted as specific EV markers (*17*–*20*). Therefore, these EV markers were identified by Western blot, and GM130 (Golgi marker) was used as a negative control. The protein concentrations per vesicle of Emb-EV and Mes-EV were 1.82 and 1.19 μg/10^{10}, respectively. We next examined EV internalization into MEFs, and Emb-EV and Mes-EV were successfully delivered into MEFs intact (fig. S2D). Considering that the cell survival rate was slightly decreased at EV concentrations above 100 μg/ml (fig. S2E), we used a final concentration of 100 μg/ml for EV-guided direct cardiac reprogramming.

Conversion of fibroblasts into iCMs

To assess the cardiac reprogramming ability of Emb-EV and Mes-EV, we performed a two-stage optimization strategy similar to the cardiomyocyte differentiation method (Fig. 1A and fig. S3A). MEFs were first exposed to Emb-EV. On day 5, the cells began forming clusters of about 100 μm in size, and the number of cell clusters increased gradually over time. Since cell cluster formation slowed considerably after 10 days, we chose day 10 as the starting point for Mes-EV treatment. After treatment with Mes-EV, cell clusters became denser and started to die after more than 5 days of treatment

(fig. S3B). Therefore, we replaced cardiac reprogramming medium (CRM) containing EVs with cardiomyocyte maturation medium (CMM) after 15 days.

Although cell clusters formed, they did not exhibit spontaneous contractions, a fundamental property of cardiomyocytes. To further optimize reprogramming medium conditions, we screened various combinations of small molecules recently described in the literature as cardiac differentiation and maturation effectors (table S2) (*21*, *22*). Treatment with EVs together with the glycogen synthase kinase-3 (GSK-3) inhibitor CHIR99021 (hereafter, C) and the tumor growth factor–β (TGF-β) inhibitor SB431542 (hereafter, S) converted MEFs into mature functional cardiomyocyte-like cells that expressed the cardiac-specific markers α-actinin, cardiac myosin heavy chain (α-MHC), and cTnT (Fig. 1B). The resulting cells also formed a large number of spontaneously beating cardiac clusters, which were not detected with small molecules alone (fig. S4, A and B). It is known that SB431542, which promotes mesenchymal-to-epithelial transition by inhibiting TGF-β signaling, and CHIR99021, which activates the Wnt pathway through inhibition of GSK-3, play pivotal roles in procedures used to promote reprogramming and induce cardiomyocyte differentiation (*23*, *24*). We confirmed that CRM containing 5% FBS and 15% knockout serum replacement (KSR) together with ascorbic acid, which is reported to enhance cellular reprogramming and cardiac maturation (*25*), was the optimal medium formulation (fig. S4C). The use of Matrigel, an extracellular matrix mimetic that indirectly influences cardiac reprogramming (*26*), also produced a further increase in iCM clusters that showed spontaneous beating behavior (fig. S4D). Last, we observed that a combination of growth factors that included basic fibroblast growth factor (bFGF) and fibroblast growth factor 10 (FGF10) increased the number of beating clusters by about 1.5-fold compared with the base (C + S) combination (fig. S4E). The overall combination of reprogramming factors and other culture conditions was crucial for achieving a direct cellular conversion process comparable to that obtained through differentiation of stem cells. With the final optimized protocol, iCMs began to contract spontaneously on day 12 after induction (movie S1), and the number of beating clusters increased in a time-dependent manner (fig. S4F). Notably, the EV-guided direct lineage conversion method in MEFs yielded a remarkable improvement in the efficiency and functionality of direct reprogramming, producing 3- and 7-fold increases compared with those achieved by conventional viral and small-molecule methods, respectively (Fig. 1, C and D, and fig. S5) (*4*, *27*).

Characterization of iCMs

Next, we assessed whether iCMs have cardiomyocyte-specific characteristics. Using immunocytochemistry (ICC) analysis, we found that iCMs resulting from EV treatment exhibited the expected expression patterns of cardiac-specific markers (α-actinin, α-MHC, and cTnT) and morphological features, displaying regularly striated sarcomeres, which form the contractile units in cardiac muscle and are structural characteristics of cardiomyocytes (Fig. 1B) (*28*). We also observed the expression of GATA binding protein 4 (GATA4), myocyte enhancer 2C (Mef2C), NK2 homeobox 5 (Nkx-2.5), and connexin43 (Cx43) proteins, which are related to cardiac development and function (Fig. 2A) (*29*). Reverse transcription quantitative polymerase chain reaction (RT-qPCR) analyses demonstrated that expression patterns of mature cardiomyocyte markers, including cTnT, ryanodine receptor 2 (Ryr2), Nkx-2.5, and GATA4, in iCMs were similar to those in neonatal cardiomyocytes (nCMs) (Fig. 2B). To further examine similarities between iCMs and endogenous nCMs from the standpoint of gene expression profiles, we performed global gene expression profiling analysis of MEFs, iCMs (days 15 and 30), and nCMs using Quant-seq 3′ mRNA sequencing. This analysis confirmed that iCMs shared similar gene expression patterns with nCMs, which became more similar as the incubation time of cells with EVs increased (Fig. 2C and fig. S6A). In particular, a Gene Ontology (GO) enrichment analysis showed that up-regulated genes are involved in heart development and maturation processes, including cardiac muscle contraction and sarcomere organization (Fig. 2D). In addition, we confirmed the signaling pathway of each gene that is differentially expressed between iCMs and nCMs using a Kyoto Encyclopedia of Genes and Genomes (KEGG) pathway enrichment analysis (fig. S6B). Together, our findings indicate that structural and molecular features of iCMs reprogrammed using the EV-guided direct lineage conversion method closely resembled those of native endogenous cardiomyocytes. We further explored the functional maturation status of iCMs by analyzing their electrophysiological and Ca^{2+} handling properties. Patch-clamp electrophysiological analyses showed that most of the iCMs exhibited ventricular-like action potentials with a maximum diastolic potential of −73.9 mV (Fig. 3A, Table 1, and movie S2). Consistent with this, ICC analyses revealed that a greater number of iCMs expressed the ventricular-specific form of myosin light chain 2 (Mlc2v) than the atrial-specific form (Mlc2a) (Fig. 3B). This result will be of particular interest for cardiac regenerative medicine since ventricular cardiomyocytes are typically lost during heart failure (*30*, *31*). We then analyzed Ca^{2+} flux during the contraction-relaxation cycle using both iCM clusters and single cells and confirmed that the mean peak [Ca^{2+}] amplitude (peak fluorescence intensity ratio, $\Delta F/F_0$) in iCMs was 3.14 ± 0.02 ($n = 6$), a value similar to those found in neonatal and ESC-derived cardiomyocytes (Fig. 3C and movie S3) (*32*), supporting the high degree of electrophysiological maturity of iCMs.

Generation through a cardiac precursor–like stage, not the iPSC stage

Normal cardiomyocyte development is known to require a cardiac precursor stage (*33*). Therefore, we assessed the expression of ISL LIM homeobox 1 (Isl1), mesoderm posterior 1 (Mesp1), GATA4, and fetal liver kinase 1 (Flk1), all of which are well-known markers of cardiac progenitor cells, in iCMs using RT-qPCR and ICC assays (Fig. 4A and fig. S7). High-level expression of these markers was observed in the early stages of EV-guided cardiac reprogramming followed by a gradual decrease over time, supporting the conclusion that iCMs passed through a cardiac precursor state. Immunostaining analysis of Ki67, a proliferation-associated nuclear protein, also confirmed that iCMs were mitotically activated (Fig. 4B). Upon further incubation under suitable differentiation conditions, we found that induced cardiac-like progenitor cells (day 15) were differentiated into smooth muscle cells or endothelial cells, with RT-qPCR and ICC analyses showing increased expression levels of genes characteristic of smooth muscle cells (CNN2, Acta2, Myh11, and α-SMA) or endothelial cells (VE-cadherin, CD31, Tie2, and PECAM) (Fig. 4, C to F). The in vivo direct cellular reprogramming paradigm for regenerative medicine is premised on the idea that cell types of interest need to be directly converted from one lineage to another without passing through an intermediate iPSC state (*1*). To determine whether the EV-guided cardiac reprogramming involves transient passage through an iPSC stage, we performed time-lapse imaging

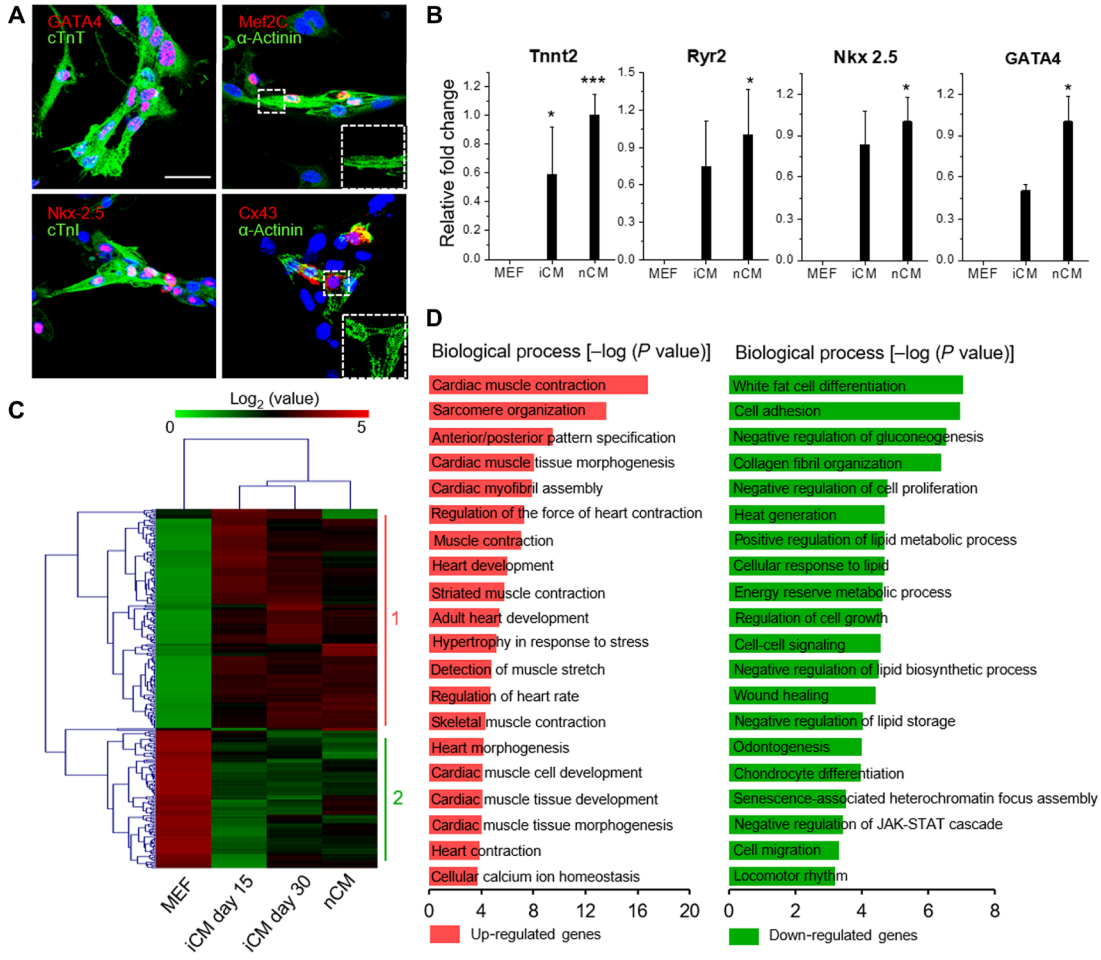

Fig. 2. Characteristics of iCMs. (**A**) Immunostaining for various markers in single cells digested from iCM beating clusters. Scale bar, 40 μm. (**B**) RT-qPCR analysis of the indicated markers in iCMs at day 30 after induction. mRNAs from MEFs and neonatal cardiomyocytes (nCMs) were used as negative and positive controls, respectively. The expression level of the corresponding markers in nCM was set to one ($n = 3$ separate experiments). Data are presented as means ± SD (***$P < 0.001$ and *$P < 0.05$ versus MEF, two-sided t test). (**C**) Heatmap illustration of Quant-seq data from MEFs, iCM beating clusters (picked on days 15 and 30), and nCMs showing up to fivefold more up-regulated or down-regulated genes in iCMs compared with MEFs. (**D**) GO term enrichment analysis of genes that displayed >5-fold change in expression in iCMs compared with MEFs. Left, up-regulated genes; right, down-regulated genes.

for up to 28 days during the reprogramming process. Using live-cell staining for alkaline phosphatase (AP), a universal marker of pluripotent cells, we found no evidence for pluripotency during the entire reprogramming process but found high-level AP expression in ESCs (Fig. 4, G and H). RT-qPCR time-course analysis also showed no expression of pluripotency genes, including Nanog and Rex1, during cardiac reprogramming (Fig. 4I). Together, these findings provide clear evidence that iCMs were generated via the cardiac precursor stage without passing through an iPSC stage. It has been shown that cardiac progenitor cells have substantially higher rates of engraftment in unfavorable transplantation environments compared with stem cells and may also assist in angiogenesis and cardiomyocyte regeneration (*34*). Thus, even from the standpoint of typical cell transplant–based approaches, cardiac reprogramming via a cardiac precursor–like stage can be beneficial for in vivo applications.

Analysis of EV miRNAs

Because of the ability of a single miRNA family to concurrently regulate multiple effectors of pathways yielding a broad range of biological processes, recently, EV miRNAs are expecting to play unique and essential roles in various pathophysiological processes via EV-mediated intercellular communication (*8*, *35*). To screen for EV miRNAs and their target genes, we performed a comparative functional analysis of miRNA profiles for both Emb-EV and Mes-EV by searching the public GO database. A number of miRNAs in Emb-EV and Mes-EV were associated with chromatin remodeling and cardiac development (Fig. 5, A and B). On the basis of calculations of read counts for miRNAs expressed in Emb-EV or Mes-EV relative to MEF- or ESC-derived EVs (fig. S8, A and B), we found that expression levels of the miR-290 cluster, miR-302-367 cluster, and miR-200, which are involved in pluripotency (*36*), mesoderm induction (*37*), and somatic reprogramming (*38*), respectively, were particularly high in Emb-EV. In addition, miR-1 and miR-133, which play key roles in cardiac differentiation and development and regulation of cardiac muscle contraction and relaxation (*39*), stood out as highly elevated miRNAs in Mes-EV. This provides strong evidence that EVs separated from ESCs undergoing the differentiation process were enriched for miRNAs involved in both initiating somatic cell reprogramming

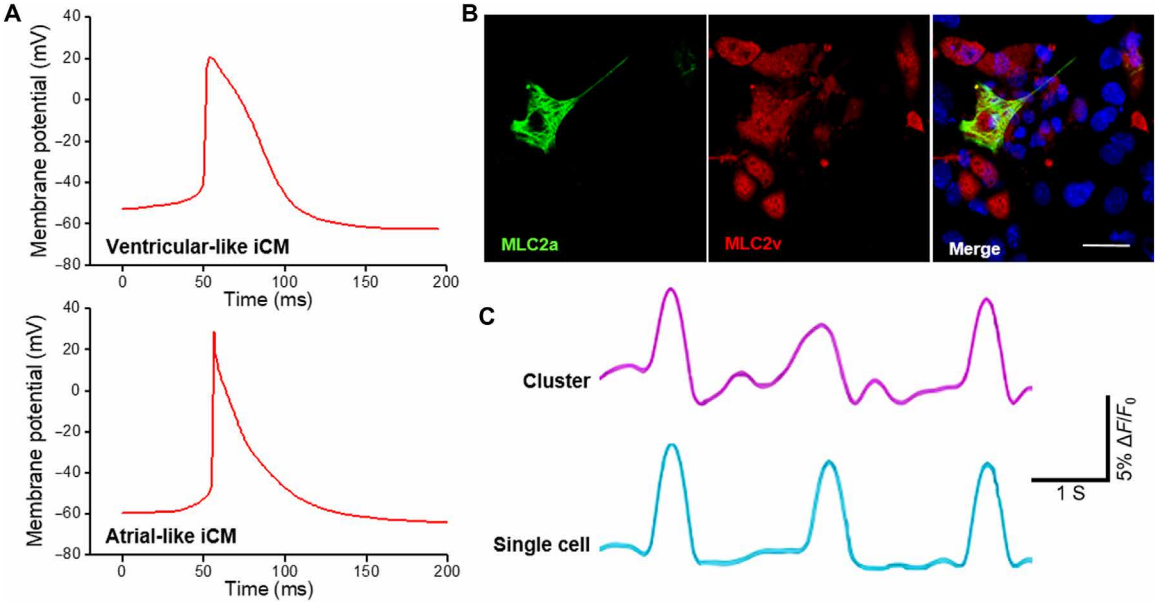

Fig. 3. Contracting iCMs generated by EVs exhibit typical cardiac Ca^{2+} flux and electrophysiological features. (**A**) Representative action potentials of iCMs; transmembrane potential in millivolts. See also Table 1. (**B**) Immunostaining for MLC2v and MLC2a in single cells digested from iCM beating clusters at day 25. Scale bar: 30 μm. (**C**) Ca^{2+} flux in iCMs at day 25 after induction. Ca^{2+} traces; transients of one cluster and a single cell. See also movie S3.

Table 1. Action potentials of iCMs. Action potential parameters of iCMs, including action potential amplitude (APA), maximum upstroke velocity (dv/dtMax), beating frequency (Freq), maximum diastolic potential (MDP), and action potential duration (APD) at the 90% repolarization level (APD90).

Cell type	A.1.1. APA (mV)	A.1.2. dv/dtMax (V/s)	A.1.3. Freq (Hz)	A.1.4. MDP (mV)	A.1.5. APD90 (ms)
V-like ($n = 10$)	87.3 ± 5.9	48.8 ± 9.5	1.6 ± 0.3	−73.9 ± 2.7	59.6 ± 21.0
A-like ($n = 4$)	81.1 ± 5.3	40.6 ± 15.8	2.6 ± 0.9	−69.8 ± 4.1	49.3 ± 10.2

and driving cardiac differentiation. Thus, sequential treatment with Emb-EV and Mes-EV allowed rapid and highly efficient direct conversion of somatic fibroblasts to mature functional iCMs. To identify key miRNAs responsible for EV-guided cardiac reprogramming, miR-291 and miR-1, which are the most frequently expressed ones in Emb-EV and Mes-EV, respectively, were silenced with each anti-miRNA during the reprogramming process. It has been known that the miR-290 family related to the Janus kinase (JAK)/signal transducer and activator of transcription 3 (STAT3) pathway and miR-1a linked to notch signaling are overexpressed and play essential roles in regulating cardiac development and reprogramming (*40*). As shown in fig. S8C, the number of beating clusters was notably reduced in the group in which one of the miRNAs was silenced. The spontaneously beating clusters were hardly founded when the function of both miRNAs was removed, indicating that miR-291 and miR-1 are critical players in EV-guided cardiac reprogramming. In contrast, miRNAs involved in somatic reprogramming or cardiac development were barely detectable in EVs derived from unprocessed ESCs or cardiomyocytes. Thus, these cells failed to produce iCMs even with our optimized treatment protocol (Fig. 5C). These results indicate that the EVs derived from stem cells and myocardial cells, which lie at the beginning and terminal stages of differentiation, respectively, cannot support direct cellular reprogramming. Together, it is reasonable to infer that cardiac reprogramming factors are generated by cells that are undergoing the cardiac differentiation process and are exported in EVs.

In vivo therapeutic efficacy of EVs for cardiac repair after myocardial infarction

To evaluate in vivo therapeutic efficiency of Emb-EV and Mes-EV against myocardial infarction (MI), EVs were administrated intramyocardially in a mouse MI model induced by ligation of the left anterior descending (LAD) coronary artery. Because of the limitation in forming the same conditions as the optimized in vitro reprogramming environment, Emb-EV and Mes-EV (EVs) were cotreated after MI induction. One week after treatment, morphological and histological examinations were carried out to assess the therapeutic effects of EVs. By using 2,3,5-triphenyltetrazolium chloride (TTC), the measurement of infarct size confirmed that the ischemic region was significantly reduced in the EV-treated group (Fig. 6A). The EV treatment also markedly attenuated cardiac apoptosis as assessed by terminal deoxynucleotidyl transferase–mediated deoxyuridine triphosphate nick end labeling (TUNEL) assay (Fig. 6B). To verify collagen deposit in the myocardial fibrosis area, cardiac tissues were stained with Masson's trichrome. The fibrotic area of the EV-treated group was decreased notably compared to that of the MI group (Fig. 6C). After 4 weeks of treatment, the functional outcomes of infarcted myocardium were evaluated. First, the proangiogenic

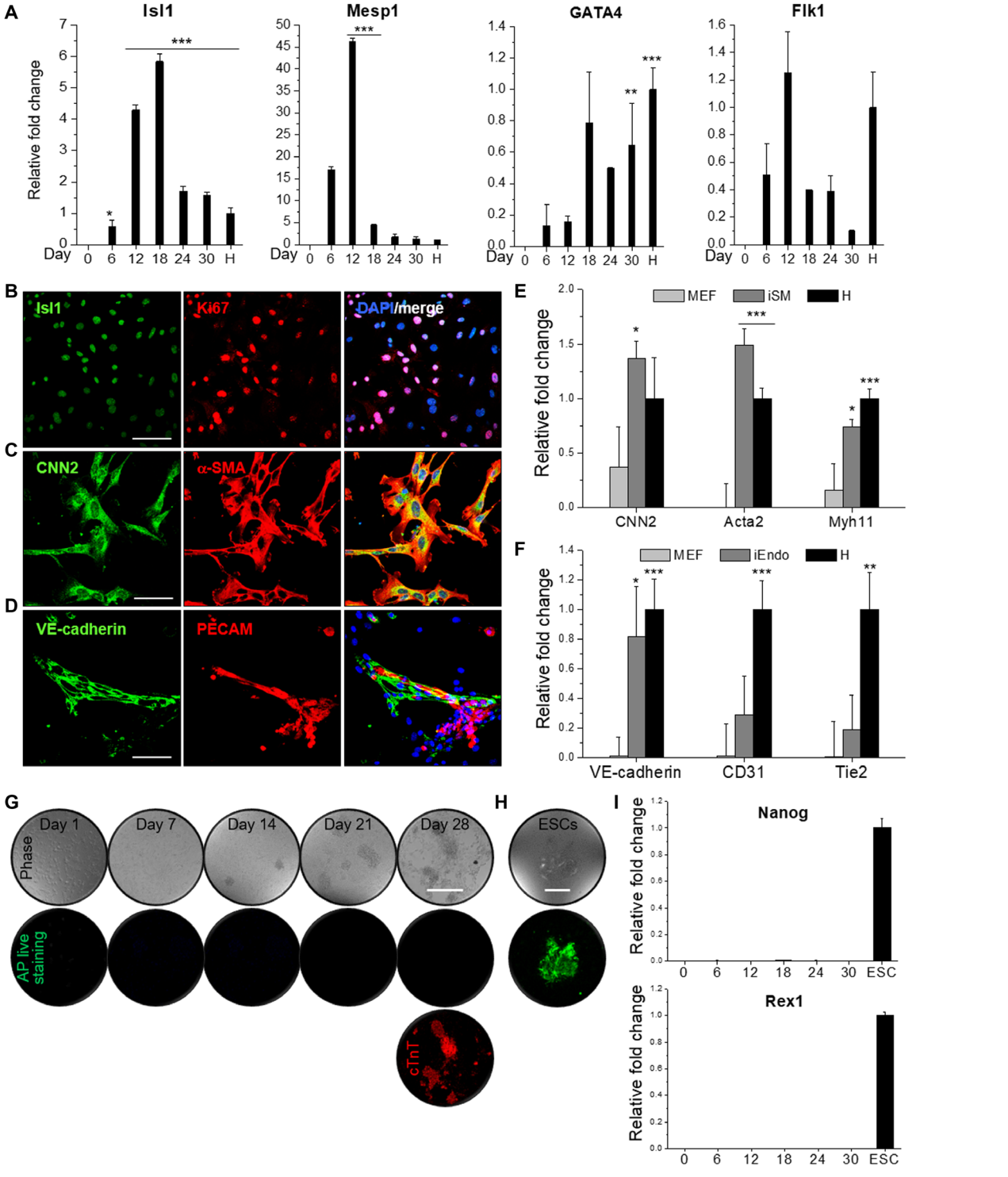

Fig. 4. Generation of iCMs via a cardiac precursor–like stage, but not via iPSCs. (**A**) Time-course analysis of cardiac precursor marker expression by RT-qPCR. "H" represents mRNA from the heart at embryonic day 13.5 (positive control) ($n = 3$ separate experiments). (**B**) Immunostaining for the markers Isl1 and Ki67 in single cells digested from clusters at day 15 after induction. (**C** and **D**) Continuous culture of Isl1$^+$ cells in either smooth muscle cell differentiation medium or endothelial cell differentiation medium for an additional 2 weeks produced Cnn2$^+$/α-SMA$^+$ cells (C) and VE-cadherin$^+$/PECAM$^+$ cells (D), respectively. (**E** and **F**) Quantitative RT-PCR analysis of the indicated markers in induced smooth muscle cells (iSMs) (E) or induced endothelial cells (iEndos) ($n = 3$ separate experiments) (F). (**G**) Phase-contrast (top) and fluorescence microscopy (bottom) time-lapse images of alkaline phosphatase (AP) live-stained iCMs generated from MEFs. iCMs were immunostained for cTnT (red) on day 28. (**H**) AP live staining of undifferentiated ESCs (positive control). (**I**) RT-qPCR analysis showing the time course of the expression of the pluripotency markers Nanog and Rex1 ($n = 3$ separate experiments). All data are presented as means ± SD (***$P < 0.001$, **$P < 0.01$, and *$P < 0.05$, two-sided t test). Scale bars, 100 μm (B to D), 300 μm (G), and 200 μm (H).

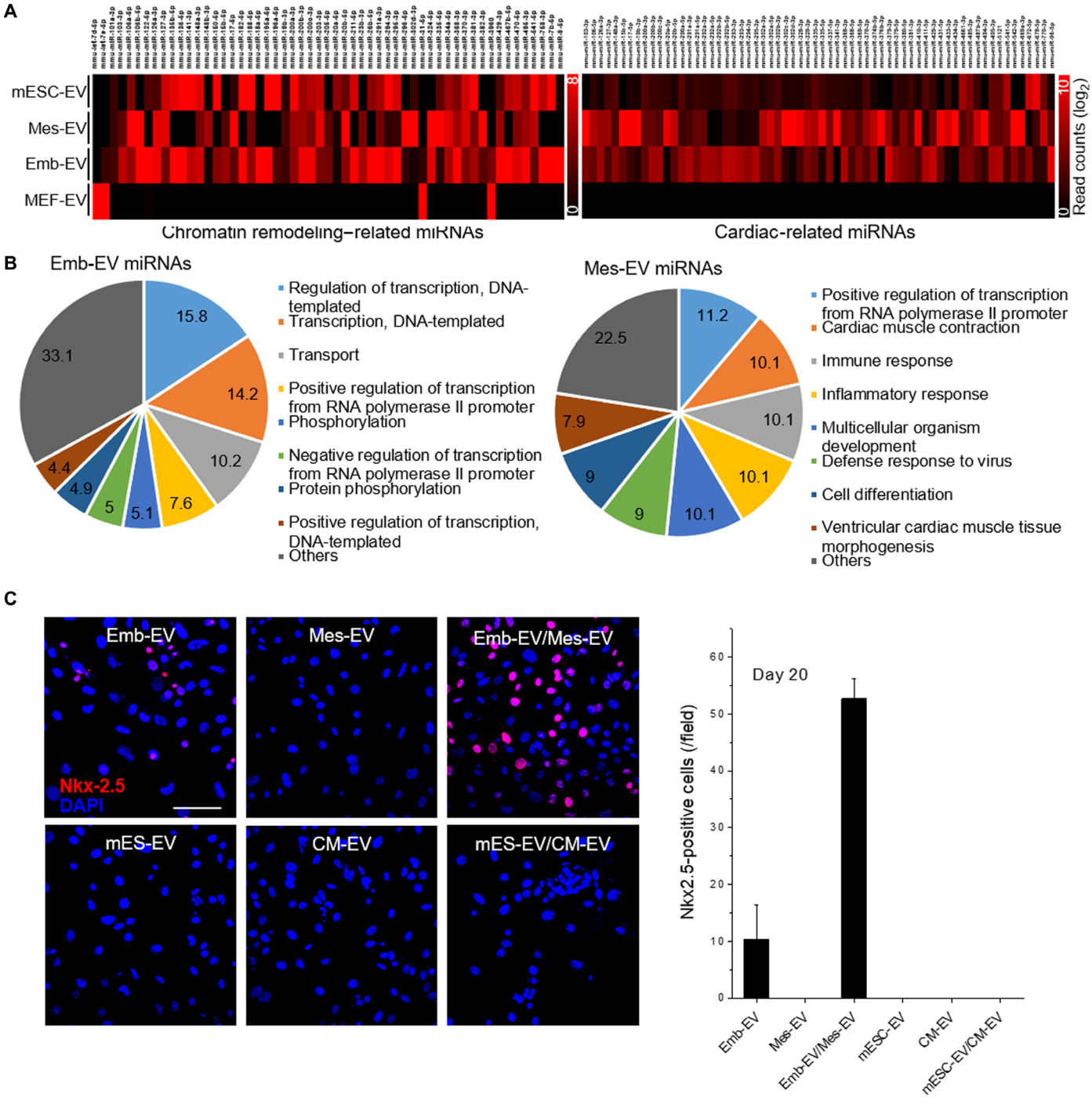

Fig. 5. Analysis of EV miRNAs from Emb-EV and Mes-EV. (**A**) Heatmaps of chromatin remodeling–related miRNAs and cardiogenesis-related miRNAs from MEF-EV, Emb-EV, Mes-EV, and mESC-EV. (**B**) GO biological process classification of Emb-EV miRNAs and Mes-EV miRNAs. (**C**) Immunostaining for Nkx-2.5 in the groups treated with EVs derived from mESCs and cardiomyocytes under the same culture conditions at day 20. Emb-EV/Mes-EV was used as a positive control. Scale bar, 100 μm.

activity induced by the EV treatment was observed by immunofluorescence staining with CD31 (Fig. 6D and fig. S9). The microvessel density was about 1.79-fold higher in the EV-treated heart than in the MI heart. Cy5-labeled EVs were still observed between the muscles and microvessels expressing cTnT and CD31 after 4 weeks of treatment. Because of the structural characteristics of the beating heart, a rapid and significant mechanical loss of implanted cells remains an obstacle to be overcome in myocardial cell therapy. Thus, this long retention ability of EVs in the beating heart could be an excellent advantage in cardiac therapy (*41*, *42*). As expected, when the optimized reprogramming protocol was applied to mouse adult cardiac fibroblasts (MCFs) in vitro, cTnT-positive cells were observed

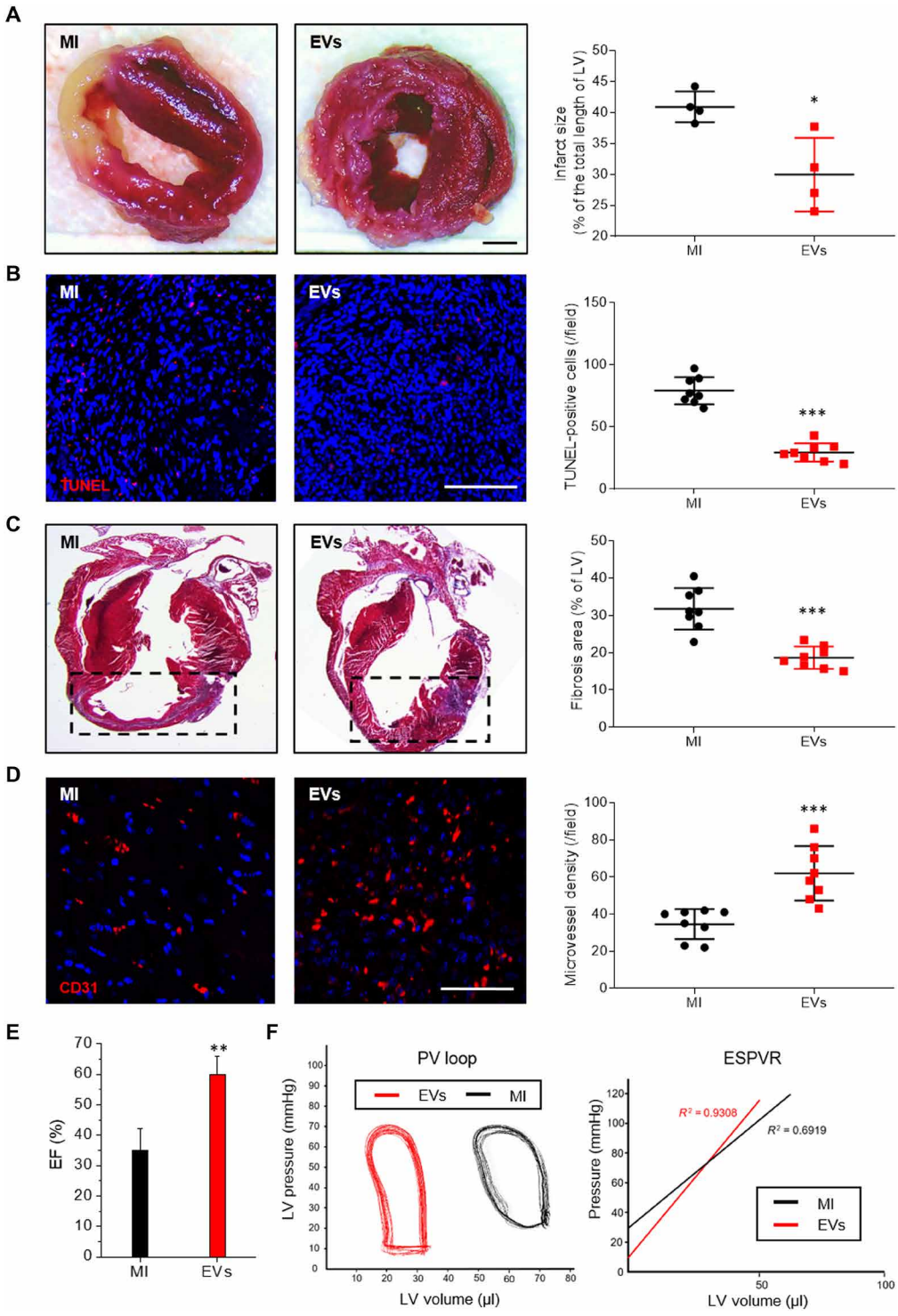

Fig. 6. In vivo therapeutic efficacy of EVs after MI. (**A**) Representative photo and column scatter plot of infarct size determined through TTC staining. The infarct size (%) was calculated as the ratio of the infarcted area (pale) to the risk area (deep red). (**B**) TUNEL assay (TUNEL-positive cells, pink; DAPI, blue) on day 7 following MI. (**C**) Masson's trichrome staining of cardiac sections 1 week after infarction (collagen fibers, light blue; muscle fibers, red). (**D**) Immunofluorescence staining for CD31 at week 4 after MI (CD31-positive microvessels, red; DAPI, blue). (**E**) Ejection fraction. (**F**) Representative pressure-volume loop (left) and end-systolic pressure-volume relationship (ESPVR) (right). All data are presented as means ± SD (***$P < 0.001$, **$P < 0.01$, and *$P < 0.05$). Scale bars, 1 mm (A), 100 μm (B), and 50 μm (D).

at day 20 (fig. S10, A and B). On the other hand, cTnT-positive cells could not be found in the group treated with heat-inactivated EVs (~90°C) or human embryonic kidney (HEK) 293–derived EVs, which are commonly used for EV studies due to their high yield. To further confirm EV-guided direct reprogramming in the heart, we injected MCFs expressing green fluorescent protein (GFP-CFs) intracardially together with EVs and performed immunofluorescence staining in mice hearts at 3 weeks after the treatment (fig. S10C). The immunohistochemistry (IHC) data showed that GFP-CFs expressed the cardiac-specific markers including GATA4 and cTnT and formed a sarcomere-like structure, supporting the hypothesis that EVs have the potential to directly reprogram cardiac fibroblasts into iCMs in vivo. Together, these results support the hypothesis that EVs separated in the process of differentiating from stem cells into cardiomyocytes can induce the recovery of MI, which is accompanied by increased expression of cardiomyocyte-specific proteins. Moreover, EVs conferred the improvement of degraded cardiac function after MI (Fig. 6, E and F, and fig. S11). Millar catheterization was used for the measurement of cardiac function based on pressure-volume relations. Compared to the MI group, the EV-treated group improved load-dependent parameters including ejection fraction and end-systolic/end-diastolic volumes, as well as load-independent parameters such as end-systolic elastance (ESP/ESV slope, ESPVR). Together, these results suggest the possibility of using the EV-guided cell reprogramming method for exploiting EVs as potential therapeutic tools to be used for heart repair.

Collectively, we showed that EVs derived from ESCs undergoing differentiation toward cardiomyocytes promote direct reprogramming of embryonic fibroblasts into mature functional iCMs. The EV-guided nonviral direct lineage conversion protocol described here is safe, rapid, and remarkably efficient, with reprogramming efficiencies reaching greater than 60%. In addition, as natural nanocarriers for small molecules, EVs also offer pharmaceutically developable formulations for in vivo direct cell conversion. Although these findings highlight the feasibility of using EVs to induce target cells into specific cell fates, detailed mechanisms of underlying signaling and epigenetic pathways require further investigation. Unlike virus-mediated transgene expression systems, which require precise knowledge and screening for individual reprogramming molecules that define target cell identity, EV-guided direct cell conversion methods, in which EVs are naturally equipped with multiple regulators, can provide a general, more readily accessible platform for broadly generating a variety of specialized somatic cells.

MATERIALS AND METHODS

Mouse ESC culture

E14tg2a (American Type Culture Collection) cells were routinely maintained in serum-containing mouse ESC (mESC) culture medium on 0.1% gelatin–coated 100-mm culture plate without feeder cells and passaged every 3 days using TrypLE Express Enzyme (Thermo Fisher Scientific). The culture medium consisted of EmbryoMax Dulbecco's modified Eagle's medium (DMEM), 10% ESC-qualified FBS, 1% nucleosides, 1% penicillin-streptomycin, 1% nonessential amino acid (NEAA), 1% L-Gln, 1% 2-mercaptoethanol, and mLIF medium supplement (1000 U/ml; Merck Millipore). mESCs were used after at least three passages before starting differentiation, and all cell cultures were routinely tested for mycoplasma contamination using the MycoAlert Kit (Lonza).

Differentiation of mESCs into cardiomyocytes using a serum-free and 2D culture system

The differentiation of mESCs into cardiomyocytes was performed as described previously with some modifications (*12*, *43*, *44*). The timeline scheme indicating medium and supplements used for differentiating mESCs to cardiomyocytes is shown in fig. S1A. All media were prepared in a sterile hood, filtered through a 0.22-μm Stericup (Merck Millipore), and stored in 4°C refrigeration. Serum-free differentiation (SFD) medium consisted of IMDM-F12 [75:25 mixtures of Iscove's modified Dulbecco's medium (IMDM) and Ham's F12 medium] (Thermo Fisher Scientific), 0.5% N-2 supplement (Thermo Fisher Scientific), 0.5% B-27 supplement without retinoic acid (Thermo Fisher Scientific), and 0.05% bovine serum albumin (BSA) (Sigma-Aldrich). Immediately before use with cells, 4.5×10^{-4} M MTG (Sigma-Aldrich), 2i (0.75 μM CHIR99021; Tocris), 0.25 μM PD0325901 (Sigma-Aldrich), and ascorbic acid (Sigma-Aldrich) were added to a final concentration of 0.5 mM. To seed ESCs, the cells were gently washed once with phosphate-buffered saline (PBS) at room temperature. Then, 1 ml of TrypLE enzyme was added and incubated at 37°C for 2 min. Cell dissociation was stopped by adding 9 ml of mESC media containing serum, and the cells were gently lifted from the plate with a pipet aid and then spun down at 125*g* for 5 min. The cells were resuspended, transferred to a 10-cm petri dish with a 10-ml cell suspension at a concentration of 2×10^4 cells/ml, and maintained at 37°C in 21% O_2 and 5% CO_2. After 48 hours, petri dish was tilted and washed with 5 ml of room temperature sterile PBS to collect the embryoid bodies, and then 15 ml of cell suspension was transferred to a conical tube and spun down to 125*g* for 3 min. The supernatant was separated to separate EVs, and the embryoid bodies were gently resuspended in 10 ml of SFD media without 2i and transferred to a new 10-cm petri dish. After another 48 hours, embryoid bodies were collected in the same manner, and then 15 ml of cell suspension was transferred to a sterile conical tube and spun down to 125*g* for 3 min. The supernatant was separated for EVs, and the embryoid bodies were dissociated by incubating for 2 min at 37°C with 1 ml of TrypLE enzyme. After gentle resuspension with a P1000 pipetman, the same volume of 4°C 10% FBS-PBS was added and spun down to 250*g* for 3 min. The cells were washed twice with room temperature PBS, resuspended in 2i-free SFD media, and seeded in a 10-cm culture dish coated with 0.1% gelatin. In addition, activin A (5 ng/ml), bone morphogenetic protein 4 (BMP4; 0.5 ng/ml), and vascular endothelial growth factor (VEGF; 5 ng/ml) were treated for 2 days for mesodermal induction (all from R&D Systems). After mesodermal induction, the medium was saved for EVs and the cells were exposed to StemPro-34 serum-free medium (Thermo Fisher Scientific), 0.5 mM ascorbic acid, VEGF (5 ng/ml), bFGF (10 ng/ml; R&D Systems), and FGF10 (5 ng/ml; R&D Systems) to induce cardiac maturation. The media were changed every other day.

EV separation

Sequential ultracentrifugation method was chosen because it was necessary to separate EVs from a large volume of cell culture solution and obtain pure EVs unmixed with other separation reagents. However, it should be noted that other components such as protein aggregates and lipoproteins can be precipitated at the bottom of the tube under a certain centrifugal force. Therefore, attention should be paid to the centrifugation conditions to avoid EV contamination. Separation of EVs from the differentiation medium was carried out

as previously described by Thery *et al.* (*45*) and reviewed by others (*46*). The EVs present in the medium from the first stage of differentiation to the stage before the mesodermal induction stage and the medium from the mesodermal induction stage were named Emb-EV and Mes-EV, respectively. Specifically, EVs derived from the culture medium on days 0 to 2 when serum-free 2D differentiation started are called Emb-EVs, and EVs isolated from the media on days 4 to 6 are called Mes-EVs (fig. S1A). The medium of each stage was centrifuged at 300*g* for 10 min to separate the remaining cells (set to maximum acceleration and deceleration rate in Avanti J-E with fixed-angle JA-20 rotor, Beckman Coulter). Subsequently, dead cells and cell debris were separated by centrifugation at 2000*g* for 10 min and 10,000*g* for 30 min, respectively. After three successive centrifugation steps, the supernatant was filtered and concentrated with the 10K Amicon Ultra-15 Centrifugal Filter Unit (Merck). The supernatant containing EVs was separated and centrifuged at 150,000*g* for 90 min (set to maximum acceleration and deceleration rate in Optima XE-100 with fixed-angle Type 70 Ti rotor, Beckman Coulter). The EV pellets were washed once with PBS and then spun down to 150,000*g* for 90 min to separate EVs. Last, EV pellets were measured for concentration via bicinchoninic acid (BCA) assay and resuspended in PBS. The entire process of EV separation was performed at 4°C, and the resuspended EVs in PBS were aliquoted into appropriate amounts and stored at −80°C.

Characterization of EVs

The DLS method is characterized by providing the most reliable data when one type of particle is present in suspension, but since it is optimized to measure particles in the 1-nm to 6-μm range, we measured the size of EVs using DLS (Zetasizer Nano S, Malvern Instruments, UK). After transferring 100 μg of EVs resuspended in 1 ml of PBS to an ultraviolet-transparent cuvette (ZEN0040, Malvern Instruments, UK), the size distribution plot with *x* and *y* axes showing the distribution of estimated particle diameter (nm) and the number of particles (percent), respectively, was analyzed with software. For TEM analysis, EVs were fixed in 2% paraformaldehyde (PFA) solution overnight. The EV solution was centrifuged for 30 min at 150,000*g* and then resuspended in absolute ethanol. Two microliters of EV suspension was transferred onto Formvar carbon–coated electron microscopy grids (Electron Microscopy Sciences). The grid was contrasted with 1% uranyl acetate solution for 1 min and then examined using TEM (Tecnai F20 G2). For EV marker analysis, EVs were quantitated by BCA protein assay, electrophoresed with 8% SDS–polyacrylamide gel electrophoresis gel, and transferred to polyvinylidene difluoride membrane (Millipore). The membrane containing proteins was blocked with 5% skim milk for 30 min at room temperature. Subsequently, the membrane was stained using 1:200 CD63 (SC-15363, Santa Cruz Biotechnology) and Alix (ab117600, Abcam) overnight at 4°C. The membrane was washed three times for 15 min with tris-buffered saline and 0.1% Tween 20 and incubated in a blocking solution with horseradish peroxidase (HRP)–tagged secondary antibodies for 1 hour at room temperature. The labeled proteins were visualized with the LAS-3000 Luminescent Image Analyzer (FujiFilm, Tokyo, Japan).

EV labeling and cellular uptake

The EVs separated during the differentiation process were labeled with a fluorescent dye (Flamma 675 NHS ester; BioActs, Korea). The EVs were incubated overnight at 4°C with the staining solution at a final concentration of 65 μM and washed twice to remove unattached dyes, using an airfuge (Beckman Coulter, USA). The EV pellet was resuspended in PBS buffer, and the suspension was used for examination of the cellular uptake of EVs. MEFs were seeded at a density of 3×10^5 cells in 35-mm confocal dish (Nunc), incubated at 37°C with the labeled EVs (25, 50, 100, and 200 μg/ml) for 1 and 4 hours, and then observed with a confocal microscope (Leica TCS SP6, Germany). The fluorescence intensities were quantified using an image analyzer.

Generation of iCMs

On the day before seeding MEFs, Matrigel (Corning) was coated on a six-well plate, sealed with Parafilm (Sigma-Aldrich), and stored at 4°C. The next day, MEFs were seeded at a density of 5×10^4 per well and incubated for 24 hours at 37°C in 5% O_2 and 5% CO_2. On day 0, media were replaced with fresh prewarmed CRM (*3*, *4*) at final concentrations of 2 μM SB431542, 10 μM CHIR99021, and Emb-EV (100 μg/ml). CRM was composed of knockout DMEM, 15% KSR, 5% ESC-qualified FBS, 0.5% N-2, 1% B-27 without vitamin A, 1% Glutamax, 1% NEAAs, 0.1 mM β-mercaptoethanol, and vitamin C (50 μg/ml; all from Thermo Fisher Scientific). CRM containing small molecules and EVs was changed every other day. On day 10, Emb-EV was replaced with Mes-EV (100 μg/ml), continued to culture until day 15, and then switched to cardiac maintenance media (CMM) on day 15. CMM is composed of DMEM, 5% FBS, 0.05% BSA fraction V, 1% Glutamax, 1% NEAA, 0.1 mM β-mercaptoethanol, and vitamin C (50 μg/ml; all from Thermo Fisher Scientific). Immediately before use with cells, we added basic FGF (10 ng/ml) and FGF10 (5 ng/ml) to CMM. All media were prepared in a sterile hood, filtered through a 0.22-μm Stericup (Merck Millipore), and stored in 4°C refrigeration. The medium was changed every other day, and the contracting cluster was observed from day 12. Other additions to CRM tested were 10 μM forskolin (LC Laboratories), 0.001 μM JAK inhibitor 1 (Merck Millipore), 2.5 μM parnate (Tocris), 10 μM RepSox (Selleckchem), 1 μM TTNPB (Tocris), 500 μM valproic acid (STEMCELL Technologies), and 10 μM Y-27632 (Tocris). In addition, 0.001% fibronectin (Sigma-Aldrich), 0.1% gelatin type A (Sigma-Aldrich), and 0.5% Matrigel (Corning) were tested as differentiation conditions according to the culture dish coating.

Generation of smooth muscle cells and endothelial cells

Induced smooth muscle cells (iSMs) and induced endothelial cells (iEndos) were generated following the same protocol for iCMs, except after day 15, the medium was switched into smooth muscle growth medium containing 50% IMDM and 50% F-12, supplemented with insulin (7 μg/ml), transferrin (15 μg/ml), 450 μM MTG, BSA (5 mg/ml), and platelet-derived growth factor–BB (10 ng/ml; R&D Systems). For iEndo, EGM-2 BulletKit (Lonza) with vascular endothelial growth factor A (10 ng/ml; R&D Systems) was used.

Immunofluorescence staining

iCMs were washed twice with PBS, treated with 0.25% trypsin/EDTA (Thermo Fisher Scientific), and incubated at 37°C for 2 min. The cells were resuspended gently three times with a P1000 pipette, incubated for 2 min at 37°C, placed in the same volume of 4°C 10% FBS-PBS, then gently mixed twice, and pelleted at 125*g* for 3 min. The cells were plated on a glass-bottom dish (Nunc) coated with 0.1% gelatin type A (Sigma-Aldrich) and grown for two more days. The cells were fixed with 4% PFA (Sigma-Aldrich) for 15 min at

room temperature and permeabilized with 0.1% Triton X-100 (Sigma-Aldrich) for 10 min at room temperature. Subsequently, the cells were blocked with 5% BSA for 1 hour at room temperature and stained with 1:200 mouse immunoglobulin G (IgG) α-MHC (ab50967), 1:200 mouse IgG cTnT (ab8295), 1:100 rabbit IgG cTnI (ab47003), 1:200 rabbit IgG GATA4 (ab84593), 1:200 rabbit IgG Mef2c (ab64644), 1:200 mouse IgG Nkx-2.5 (ab91196), 1:200 rabbit IgG Connexin-43 (ab11370), 1:100 polyclonal rabbit IgG MLC2v (ab79935), 1:200 monoclonal mouse IgG Ki67 (ab8191, all Abcam), 1:100 monoclonal rabbit IgG α-actinin (7H1L69, Thermo Fisher Scientific), 1:300 monoclonal mouse IgG MLC2a (#311011, Synaptic systems), 1:100 polyclonal rabbit IgG Isl1 (LS-C334676, LifeSpan BioSciences), 1:400 monoclonal mouse IgG SMA (A2547, Sigma-Aldrich), 1:100 polyclonal goat IgG Calponin 2 (sc-16607), 1:100 polyclonal goat IgG PECAM (sc-1506), or 1:100 monoclonal mouse IgG VE-cadherin (sc-9989, all Santa Cruz Biotechnology) overnight at 4°C in 1% BSA in PBS. The cells were washed twice with 1% BSA in PBS for 15 min and then incubated for 1 hour at room temperature in the dark with secondary antibodies 1:2000 Alexa Fluor 488 goat anti-mouse IgG (H&L), 1:2000 Alexa Fluor 488 donkey anti-rabbit IgG (H&L), 1:2000 Alexa Fluor 647 goat anti-mouse IgG (H&L), 1:2000 Alexa Fluor 647 donkey anti-rabbit IgG (H&L), 1:2000 Alexa Fluor 488 donkey anti-goat IgG (H&L), or 1:2000 Alexa Fluor 647 donkey anti-goat IgG (H&L) (all from Life Technologies) in 1% BSA in PBS. The cells were washed again as above, and nuclei were stained with DAPI (4′,6-diamidino-2-phenylindole; Sigma-Aldrich) and imaged with a TCS SP5 confocal microscope (Leica Microsystems).

Flow cytometry

The cells were detached into single-cell suspension with 0.25% trypsin/EDTA, fixed with 1% PFA for 15 min, permeabilized with 90% methanol for 15 min at 4°C, and stained using 1:200 mouse IgG α-MHC (ab15, Abcam) or 1:200 mouse IgG cTnT (ab8295) for 45 min at room temperature. Secondary staining was performed with 1:1000 Alexa Fluor 488 goat anti-mouse IgG or 1:1000 Alexa Fluor 647 goat anti-mouse IgG (all from Life Technologies) for 20 min in the dark. Mouse IgG (#31903, Thermo Fisher Scientific) was used as isotype control. The stained cells were analyzed using Guava easyCyte Flow Cytometers (Merck Millipore) with a 100-μm nozzle, and data were analyzed using FlowJo 8.6 (TreeStar).

Quantitative real-time PCR

To analyze gene expression, cells were dissociated with TrypLE Express reagent (Thermo Fisher Scientific), and pellets were stored in a deep freezer at −80°C. Total RNA from the samples at designated time points was extracted using an RNeasy Plus Mini kit with Qiashredder (QIAGEN). RNA was reverse-transcribed using the High-Capacity RNA-to-cDNA Kit (Life Technologies), and real-time qPCR was performed with PowerUp SYBR Green Master Mix (Thermo Fisher Scientific) on the StepOnePlus Real-Time PCR System (Applied Biosystems). All qPCRs were performed in triplicate. The expression data were normalized to β-actin levels and assessed using the comparative change in the threshold cycle method. Real-time PCR primer sequences are listed in table S3.

Intracellular Ca^{2+} measurement

To record calcium transients, iCMs were loaded with 2 μM Fluo-3 AM Ca^{2+} indicator (Thermo Fisher Scientific), as directed by the manufacturer, at 37°C for 20 min to allow for deesterification of the dye. After changing dye-containing media with a fresh culture media, spontaneous Ca^{2+} transients were recorded at 37°C using a BX51 fluorescence microscope (Olympus) and a time-lapse recording system (Xcellence). For the clusters of iCMs, cell-framing adapters were adjusted to record fluorescence for whole clusters and cell-free boundaries. The background fluorescence was recorded after cells were removed from the field of view at the end for normalization. The peak amplitude of calcium fluxes was defined as the difference between the baseline (average $\Delta F/F_0$ of 2 s evoked by a single action potential).

Electrophysiological analysis

A conventional whole-cell patch clamp was performed. Spontaneously beating iCMs were selected to record action potential (AP). iCMs were perfused at physiological temperature of 35° to 37°C with normal Tyrode's solution containing 145 mM NaCl, 5.4 mM KCl, 1 mM $MgCl_2$, 1.8 mM $CaCl_2$, 10 mM Hepes, and 5 mM glucose and adjusted to pH 7.4 with NaOH. Intracellular pipette solution contained 120 mM K-aspartate, 25 mM KCl, 5 mM NaCl, 10 mM Hepes, 0.1 mM EGTA, 1 mM $MgCl_2$, and 3 mM Mg–adenosine triphosphate (ATP) and was adjusted to pH 7.2 with KOH. Liquid junction potential compensation (10 mV) was applied after the experiment. Microglass patch pipettes (World Precision Instruments) were pulled using a PP-830 puller (Narishige, Japan) with resistance between 2 and 3 megohms. Axopatch 200B amplifier, Digidata 1550B AD-DA convertor, and pClamp software 11 (Axon Instruments) were used for AP recording and analysis.

Next-generation sequencing of iCMs and EVs

Quant-seq 3′ mRNA sequencing was performed for gene expression analysis of cells, and miRNA sequencing was carried out for EV analysis. The beating colonies were picked at the designated day, and total RNA was isolated using TRIzol reagent (Thermo Fisher Scientific). RNA quality was assessed with an Agilent 2100 bioanalyzer using the RNA 6000 Nano Chip for Quan-seq 3′ mRNA sequencing and the RNA 6000 Pico Chip for EV miRNA sequencing (both from Agilent Technologies). The RNA quantification was performed using the NanoDrop 2000 Spectrophotometer System (Thermo Fisher Scientific). For the construction of library, the QuantSeq 3′ mRNA-Seq Library Prep Kit (Lexogen Inc., Austria) was used for gene expression analysis, and the NEBNext Multiplex Small RNA Library Prep Kit (New England BioLabs) was used for EV miRNA sequencing according to the manufacturer's instructions. The yield and size distribution of the small RNA libraries were assessed by the Agilent 2100 Bioanalyzer instrument for the High Sensitivity DNA Assay (Agilent Technologies), and high-throughput sequences were produced by NextSeq 500 system as a way of single-end 75 sequencing (Illumina). Sequence reads were mapped by a Bowtie2 software tool to obtain a bam file (alignment file). Read counts mapped on differentially expressed genes and mature miRNA sequences were extracted from the alignment file using Bedtools (v2.25.0) and Bioconductor using R (version 3.2.2) statistical programming language (R Development Core Team, 2016). Read counts were used to determine the expression levels of miRNAs. Quantile normalization method was used for comparison between samples. Gene classification was based on searches done by DAVID (http://david.ncifcrf.gov) and Medline databases (www.ncbi.nlm.nih.gov/). For the miRNA target study, miRWalk 2.0 was performed. Hierarchical cluster analyses were carried out with Euclidean distance correlation as the

distance measurement with average linkage. Clusters and heatmaps were visualized via MeV 4.9.0. The Quant-seq data of iCMs and the EV RNA sequencing data in this study are available at the National Center for Biotechnology Information (NCBI) Gene Expression Omnibus with accession number GSE166251 (www.ncbi.nlm.nih.gov/geo/info/linking.html). For the anti-miRNA transfection, 10 days after induction of reprogramming, transfection was performed at a concentration of 50 pmol/ml of anti-miRNA using Lipofectamine according to the manufacturer's manual.

MI model and EV treatment

Surgical procedures were approved by the Institutional Animal Care and Use Committee, Catholic Kwandong University College of Medicine (No. CKU 01-2020-009), and the Association for Assessment and Accreditation of Laboratory Animal Care and were performed by the Guidelines and Regulations for Animal Care. The male C57BL/6 mice aged 12 weeks were divided into two groups: MI + PBS ($n = 8$) and MI + EV ($n = 8$). The mice were anesthetized via intraperitoneal injection of tiletamine/zolazepam (Zoletile, 30 mg/kg) and xylazine (10 mg/kg), ventilated with a volume-regulated respirator (VentElite 55-7040, Harvard Apparatus, Holliston, MA, USA), and then subjected to median sternotomy. The MI model was induced by ligation of the LAD coronary artery using a 6-0 Prolene suture (Covidien, Dublin, Ireland). After ischemia, EVs (400 ng/μl) mixed with PBS in a total volume of 10 μl were intramyocardially injected into three sites in the border zones of infarcted myocardium. Then, the muscle and skin were sutured with 4-0 Prolene suture, each. For pathological and functional analysis, mice were sacrificed at week 1 or week 4, respectively. For the in vivo reprogramming analysis, mouse cardiac fibroblasts expressing GFP (GFP-CFs) (CellBiologics, mGFP-6049) were suspended in 30 μl of PBS (1×10^6 cells) and intracardially injected with EVs using an insulin syringe. After 3 weeks of treatment, hearts were harvested from sacrificed mice and subjected to IHC analysis.

TTC stain

To measure the myocardial infarct area, isolated hearts were perfused with 1% TTC (Sigma-Aldrich, St. Louis, MO, USA) for 1 hour at 37°C and incubated in 4% formaldehyde overnight at 4°C. The heart sections were photographed with a digital camera (DIMIS M model, Anyang, Korea). The infarcted area was measured by using ImageJ software.

Histology and immunofluorescence

Longitudinal sections of a thickness of 5 μm were cut from apex to base and mounted on a glass slide. Masson's trichrome staining was examined according to standard protocols, and measurement of fibrosis area was determined by using ImageJ software. In infarcted myocardium, apoptotic and necrotic cells were determined using TUNEL Assay Kit—BrdU-Red (Abcam, Cambridge, UK, #ab66110). TUNEL assay was also performed according to the manufacturer's instructions. The TUNEL assay images were blindly captured and counted using virtual microscopy (BX51 Dot Slide; Olympus, Tokyo, Japan). To assess the relationship between transplanted EV and ischemic myocardium, IHC was examined. Sections were deparaffinized and then incubated in 1% H_2O_2 to quench endogenous peroxidase. Heart tissues were blocked for 1 hour with a mixture of 1% (w/v) BSA and 5% (v/v) horse serum and incubated in cTnT antibody (Abcam, UK, #ab8295) or CD31 antibody (Santa Cruz Biotechnology, Dallas, TX, USA, #sc1506) at a ratio of 1:200 each. After three washes with PBS, the sections were incubated with secondary antibody (Alexa Fluor 488, #ab150077; Alexa Fluor 594, #ab150116; at a ratio of 1:250 each; Abcam) for 1 hour at room temperature, mounted with DAPI, and viewed under a confocal microscope (LSM 700, Carl Zeiss, Oberkochen, Germany).

Millar catheterization

For the measurement of invasive hemodynamics, left ventricular (LV) catheterization was performed at 4 weeks after MI. A mouse pressure-volume loop catheter (SPR-839, Millar Instruments, Houston, TX, USA, #SPR-839NR) was introduced into the LV via the right carotid artery (closed-chest surgery) under anesthesia. Ventricular pressure and real-time volume loops were recorded, and all data were analyzed using LabChart v8.1.5 software (Millar).

Statistical analysis

All graphs were plotted with OriginPro 8 software package (OriginLab Corp., MA, USA). Data are presented as means ± SD. Statistical analysis was carried out by Student's t test, and a value of $P < 0.05$ was considered statistically significant.

SUPPLEMENTARY MATERIALS

Supplementary material for this article is available at https://science.org/doi/10.1126/sciadv.abj6621

View/request a protocol for this paper from *Bio-protocol*.

REFERENCES AND NOTES

1. T. Graf, T. Enver, Forcing cells to change lineages. *Nature* **462**, 587–594 (2009).
2. P. Zhou, W. T. Pu, Recounting cardiac cellular composition. *Circ. Res.* **118**, 368–370 (2016).
3. J. A. Efe, S. Hilcove, J. Kim, H. Zhou, K. Ouyang, G. Wang, J. Chen, S. Ding, Conversion of mouse fibroblasts into cardiomyocytes using a direct reprogramming strategy. *Nat. Cell Biol.* **13**, 215–222 (2011).
4. H. Wang, N. Cao, C. I. Spencer, B. Nie, T. Ma, T. Xu, Y. Zhang, X. Wang, D. Srivastava, S. Ding, Small molecules enable cardiac reprogramming of mouse fibroblasts with a single factor, Oct4. *Cell Rep.* **6**, 951–960 (2014).
5. C. E. Thomas, A. Ehrhardt, M. A. Kay, Progress and problems with the use of viral vectors for gene therapy. *Nat. Rev. Genet.* **4**, 346–358 (2003).
6. F. Anokye-Danso, C. M. Trivedi, D. Juhr, M. Gupta, Z. Cui, Y. Tian, Y. Zhang, W. Yang, P. J. Gruber, J. A. Epstein, E. E. Morrisey, Highly efficient miRNA-mediated reprogramming of mouse and human somatic cells to pluripotency. *Cell Stem Cell* **8**, 376–388 (2011).
7. T. M. Jayawardena, B. Egemnazarov, E. A. Finch, L. Zhang, J. A. Payne, K. Pandya, Z. Zhang, P. Rosenberg, M. Mirotsou, V. J. Dzau, MicroRNA-mediated in vitro and in vivo direct reprogramming of cardiac fibroblasts to cardiomyocytes. *Circ. Res.* **110**, 1465–1473 (2012).
8. P. J. Quesenberry, J. Aliotta, M. C. Deregibus, G. Camussi, Role of extracellular RNA-carrying vesicles in cell differentiation and reprogramming. *Stem Cell Res. Ther.* **6**, 153 (2015).
9. M. Lloret-Llinares, E. Karadoulama, Y. Chen, L. A. Wojenski, G. J. Villafano, J. Bornholdt, R. Andersson, L. Core, A. Sandelin, T. H. Jensen, The RNA exosome contributes to gene expression regulation during stem cell differentiation. *Nucleic Acids Res.* **46**, 11502–11513 (2018).
10. G. V. Shelke, C. Lasser, Y. S. Gho, J. Lotvall, Importance of exosome depletion protocols to eliminate functional and RNA-containing extracellular vesicles from fetal bovine serum. *J. Extracell. Vesicles* **3**, 24783 (2014).
11. K. R. Boheler, J. Czyz, D. Tweedie, H. T. Yang, S. V. Anisimov, A. M. Wobus, Differentiation of pluripotent embryonic stem cells into cardiomyocytes. *Circ. Res.* **91**, 189–201 (2002).
12. M. E. Hartman, J. R. Librande, I. O. Medvedev, R. N. Ahmad, F. Moussavi-Harami, P. P. Gupta, W. M. Chien, M. T. Chin, An optimized and simplified system of mouse embryonic stem cell cardiac differentiation for the assessment of differentiation modifiers. *PLOS ONE* **9**, e93033 (2014).
13. H. Kempf, C. Kropp, R. Olmer, U. Martin, R. Zweigerdt, Cardiac differentiation of human pluripotent stem cells in scalable suspension culture. *Nat. Protoc.* **10**, 1345–1361 (2015).
14. H. Kempf, R. Zweigerdt, Scalable cardiac differentiation of pluripotent stem cells using specific growth factors and small molecules. *Adv. Biochem. Eng. Biotechnol.* **163**, 39–69 (2018).

15. R. Kakarla, J. Hur, Y. J. Kim, J. Kim, Y. J. Chwae, Apoptotic cell-derived exosomes: Messages from dying cells. *Exp. Mol. Med.* **52**, 1–6 (2020).
16. C. Thery, M. Boussac, P. Veron, P. Ricciardi-Castagnoli, G. Raposo, J. Garin, S. Amigorena, Proteomic analysis of dendritic cell-derived exosomes: A secreted subcellular compartment distinct from apoptotic vesicles. *J. Immunol.* **166**, 7309–7318 (2001).
17. D. Kumar, D. Gupta, S. Shankar, R. K. Srivastava, Biomolecular characterization of exosomes released from cancer stem cells: Possible implications for biomarker and treatment of cancer. *Oncotarget* **6**, 3280–3291 (2015).
18. C. Raiborg, H. Stenmark, The ESCRT machinery in endosomal sorting of ubiquitylated membrane proteins. *Nature* **458**, 445–452 (2009).
19. E. Willms, H. J. Johansson, I. Mager, Y. Lee, K. E. Blomberg, M. Sadik, A. Alaarg, C. I. Smith, J. Lehtio, S. El Andaloussi, M. J. Wood, P. Vader, Cells release subpopulations of exosomes with distinct molecular and biological properties. *Sci. Rep.* **6**, 22519 (2016).
20. Y. Wu, W. Deng, D. J. Klinke 2nd, Exosomes: Improved methods to characterize their morphology, RNA content, and surface protein biomarkers. *Analyst* **140**, 6631–6642 (2015).
21. N. Cao, Y. Huang, J. Zheng, C. I. Spencer, Y. Zhang, J. D. Fu, B. Nie, M. Xie, M. Zhang, H. Wang, T. Ma, T. Xu, G. Shi, D. Srivastava, S. Ding, Conversion of human fibroblasts into functional cardiomyocytes by small molecules. *Science* **352**, 1216–1220 (2016).
22. P. Hou, Y. Li, X. Zhang, C. Liu, J. Guan, H. Li, T. Zhao, J. Ye, W. Yang, K. Liu, J. Ge, J. Xu, Q. Zhang, Y. Zhao, H. Deng, Pluripotent stem cells induced from mouse somatic cells by small-molecule compounds. *Science* **341**, 651–654 (2013).
23. X. Lian, C. Hsiao, G. Wilson, K. Zhu, L. B. Hazeltine, S. M. Azarin, K. K. Raval, J. Zhang, T. J. Kamp, S. P. Palecek, Robust cardiomyocyte differentiation from human pluripotent stem cells via temporal modulation of canonical Wnt signaling. *Proc. Natl. Acad. Sci. U.S.A.* **109**, E1848–E1857 (2012).
24. L. Marucci, E. Pedone, U. Di Vicino, B. Sanuy-Escribano, M. Isalan, M. P. Cosma, beta-catenin fluctuates in mouse ESCs and is essential for Nanog-mediated reprogramming of somatic cells to pluripotency. *Cell Rep.* **8**, 1686–1696 (2014).
25. M. A. Esteban, T. Wang, B. Qin, J. Yang, D. Qin, J. Cai, W. Li, Z. Weng, J. Chen, S. Ni, K. Chen, Y. Li, X. Liu, J. Xu, S. Zhang, F. Li, W. He, K. Labuda, Y. Song, A. Peterbauer, S. Wolbank, H. Redl, M. Zhong, D. Cai, L. Zeng, D. Pei, Vitamin C enhances the generation of mouse and human induced pluripotent stem cells. *Cell Stem Cell* **6**, 71–79 (2010).
26. Y. P. Kong, B. Carrion, R. K. Singh, A. J. Putnam, Matrix identity and tractional forces influence indirect cardiac reprogramming. *Sci. Rep.* **3**, 3474 (2013).
27. Y. Fu, C. Huang, X. Xu, H. Gu, Y. Ye, C. Jiang, Z. Qiu, X. Xie, Direct reprogramming of mouse fibroblasts into cardiomyocytes with chemical cocktails. *Cell Res.* **25**, 1013–1024 (2015).
28. J. C. Sparrow, F. Schock, The initial steps of myofibril assembly: Integrins pave the way. *Nat. Rev. Mol. Cell Biol.* **10**, 293–298 (2009).
29. I. ten Velde, B. de Jonge, E. E. Verheijck, M. J. van Kempen, L. Analbers, D. Gros, H. J. Jongsma, Spatial distribution of connexin43, the major cardiac gap junction protein, visualizes the cellular network for impulse propagation from sinoatrial node to atrium. *Circ. Res.* **76**, 802–811 (1995).
30. M. Chiong, Z. V. Wang, Z. Pedrozo, D. J. Cao, R. Troncoso, M. Ibacache, A. Criollo, A. Nemchenko, J. A. Hill, S. Lavandero, Cardiomyocyte death: Mechanisms and translational implications. *Cell Death Dis.* **2**, e244 (2011).
31. Z. Lin, W. T. Pu, Strategies for cardiac regeneration and repair. *Sci. Transl. Med.* **6**, 239 (2014).
32. V. Robert, P. Gurlini, V. Tosello, T. Nagai, A. Miyawaki, F. Di Lisa, T. Pozzan, Beat-to-beat oscillations of mitochondrial [Ca2+] in cardiac cells. *EMBO J.* **20**, 4998–5007 (2001).
33. B. Zhou, Q. Ma, S. Rajagopal, S. M. Wu, I. Domian, J. Rivera-Feliciano, D. Jiang, A. von Gise, S. Ikeda, K. R. Chien, W. T. Pu, Epicardial progenitors contribute to the cardiomyocyte lineage in the developing heart. *Nature* **454**, 109–113 (2008).
34. C. Mauritz, A. Martens, S. V. Rojas, T. Schnick, C. Rathert, N. Schecker, S. Menke, S. Glage, R. Zweigerdt, A. Haverich, U. Martin, I. Kutschka, Induced pluripotent stem cell (iPSC)-derived Flk-1 progenitor cells engraft, differentiate, and improve heart function in a mouse model of acute myocardial infarction. *Eur. Heart J.* **32**, 2634–2641 (2011).
35. J. M. Aliotta, F. M. Sanchez-Guijo, G. J. Dooner, K. W. Johnson, M. S. Dooner, K. A. Greer, D. Greer, J. Pimentel, L. M. Kolankiewicz, N. Puente, S. Faradyan, P. Ferland, E. L. Bearer, M. A. Passero, M. Adedi, G. A. Colvin, P. J. Quesenberry, Alteration of marrow cell gene expression, protein production, and engraftment into lung by lung-derived microvesicles: A novel mechanism for phenotype modulation. *Stem Cells* **25**, 2245–2256 (2007).
36. R. L. Judson, T. S. Greve, R. J. Parchem, R. Blelloch, MicroRNA-based discovery of barriers to dedifferentiation of fibroblasts to pluripotent stem cells. *Nat. Struct. Mol. Biol.* **20**, 1227–1235 (2013).
37. A. Rosa, F. M. Spagnoli, A. H. Brivanlou, The miR-430/427/302 family controls mesendodermal fate specification via species-specific target selection. *Dev. Cell* **16**, 517–527 (2009).
38. G. Wang, X. Guo, W. Hong, Q. Liu, T. Wei, C. Lu, L. Gao, D. Ye, Y. Zhou, J. Chen, J. Wang, M. Wu, H. Liu, J. Kang, Critical regulation of miR-200/ZEB2 pathway in Oct4/Sox2-induced mesenchymal-to-epithelial transition and induced pluripotent stem cell generation. *Proc. Natl. Acad. Sci. U.S.A.* **110**, 2858–2863 (2013).
39. J. F. Chen, E. M. Mandel, J. M. Thomson, Q. Wu, T. E. Callis, S. M. Hammond, F. L. Conlon, D. Z. Wang, The role of microRNA-1 and microRNA-133 in skeletal muscle proliferation and differentiation. *Nat. Genet.* **38**, 228–233 (2006).
40. C. Piubelli, V. Meraviglia, G. Pompilio, Y. D'Alessandra, G. I. Colombo, A. Rossini, microRNAs and cardiac cell fate. *Cell* **3**, 802–823 (2014).
41. W. Hudson, M. C. Collins, D. deFreitas, Y. S. Sun, B. Muller-Borer, A. P. Kypson, Beating and arrested intramyocardial injections are associated with significant mechanical loss: Implications for cardiac cell transplantation. *J. Surg. Res.* **142**, 263–267 (2007).
42. C. J. Teng, J. Luo, R. C. Chiu, D. Shum-Tim, Massive mechanical loss of microspheres with direct intramyocardial injection in the beating heart: Implications for cellular cardiomyoplasty. *J. Thorac. Cardiovasc. Surg.* **132**, 628–632 (2006).
43. I. Kokkinopoulos, H. Ishida, R. Saba, S. Coppen, K. Suzuki, K. Yashiro, Cardiomyocyte differentiation from mouse embryonic stem cells using a simple and defined protocol. *Dev. Dyn.* **245**, 157–165 (2016).
44. S. J. Kattman, A. D. Witty, M. Gagliardi, N. C. Dubois, M. Niapour, A. Hotta, J. Ellis, G. Keller, Stage-specific optimization of activin/nodal and BMP signaling promotes cardiac differentiation of mouse and human pluripotent stem cell lines. *Cell Stem Cell* **8**, 228–240 (2011).
45. C. Thery, S. Amigorena, G. Raposo, A. Clayton, Isolation and characterization of exosomes from cell culture supernatants and biological fluids. *Curr. Protoc. Cell Biol.*, **Chapter 3**, Unit 3.22, (2006).
46. P. Li, M. Kaslan, S. H. Lee, J. Yao, Z. Gao, Progress in exosome isolation techniques. *Theranostics* **7**, 789–804 (2017).

Acknowledgments

Funding: This study was supported by the National Research Foundation of Korea (NRF) (grants NRF-2019R1A2C2010408 and NRF-2020R1C1C1013535) by the Korea government and Intramural Research Program of Korea Institute of Science and Technology (KIST). **Author contributions:** Conceptualization: H.K., I.C.K., and S.H.K. Methodology: S.-W.K., S.-H.M., Y.Y., I.C.K., and S.H.K. Visualization: H.K., B.-W.S., S.-J.P., S.W.C., and H.M. Funding acquisition: B.-W.S., K.-C.H., and S.H.K. Supervision: I.C.K. and S.H.K. Writing—original draft: H.K. Writing—review and editing: H.K., B.-W.S., and S.H.K. **Competing interests:** The authors declare that they have no competing interests. **Data and materials availability:** All data needed to evaluate the conclusions in the paper are present in the paper and/or the Supplementary Materials.

Submitted 26 May 2021
Accepted 31 December 2021
Published 25 February 2022
10.1126/sciadv.abj6621